Proceedings of ASME Turbo Expo 2011
GT2011
June 6-10, 2011, Vancouver, British Columbia, Canada

GT2011-45402

MULTI-OBJECTIVE OPTIMIZATION OF FILM-COOLING HOLES CONSIDERING HEAT TRANSFER AND AERODYNAMIC LOSS

Ki-Don Lee, Sun-Min Kim and Kwang-Yong Kim
Dept. of Mechanical Engineering
Inha University
Incheon, Republic of Korea
kykim@inha.ac.kr

ABSTRACT

In the present work, multi-objective shape optimization of a row of laidback fan shaped film cooling holes has been performed using a hybrid multi-objective evolutionary approach in order to achieve an acceptable compromise between two competing objectives, i.e., enhancement of the film cooling effectiveness and reduction of the aerodynamic loss. In order to perform comprehensive optimization of film-cooling hole shape, the injection angle of the hole, the lateral expansion angle of the diffuser, the forward expansion angle of the hole and the pitch to hole diameter ratio, are chosen as design variables. Forty experimental designs within design spaces are selected by Latin hypercube sampling method. The response surface approximation method is used to construct the surrogate with objective function values for the experimental designs calculated through Reynolds-averaged Navier-Stokes analysis. The shear stress transport turbulence model is used as a turbulence closure. The optimization results are processed by the Pareto-optimal method. The Pareto optimal solutions are obtained using a combination of the evolutionary algorithm NSGA-II and a local search method. The optimum designs are grouped by k-means clustering technique and the six optimal points selected in the Pareto optimal solutions are evaluated by numerical analysis. The different trends in the variations of the design variables for each blowing ratios were found, and the optimum designs show enhanced objective function values.

NOMENCLATURE

A_m	area of main channel
D	film-cooling hole diameter
F	objective function
KE	kinetic energy
L	film-cooling hole length
M	Blowing ratio ($=\rho_c V_c$)/($\rho_\infty V_\infty$)
m	mass flux (=ρV)
P	hole-to-hole pitch
p	pressure
T	temperature
V	velocity
W	width of hole exit side
x, y, z	coordinates
y	distance from the wall
$y+$	y in law of the wall coordinate
α	injection angle of hole
β	lateral expansion angle of cooling hole diffuser
γ	forward expansion angle of cooling hole diffuser
ρ	density
η	film-cooling effectiveness: $(T_{aw}-T_\infty)/(T_c-T_\infty)$
η_l	laterally averaged film-cooling effectiveness
η_s	spatially averaged film-cooling effectiveness

Subscript

AL	aerodynamic loss
aw	adiabatic wall
c	coolant
FCE	film-cooling effectiveness
∞	free stream, main channel
0	total
1	reference plane
2	mixing plane

INTRODUCTION

In the development of up-to-date gas turbine, there has been substantial effort focused on increasing the inlet temperature of the turbine to increase the thermal efficiency and the specific thrust. Therefore, the development of effective cooling technique is recognized as an essential part in the gas

turbine research. Among many others, film-cooling technique [1] has been widely used for gas turbine blades as the very important alternative. In this technique, coolant air is injected on the surface to provide a protective layer which helps in maintaining the external walls at an acceptable temperature level, thus protecting the turbine blade from failure. However, film-cooling inevitably results in increasing the aerodynamic loss due to the interaction of the mainstream hot gas with the coolant jet. In the design of the hole geometry, thus, the aerodynamic loss as well as the film-cooling effectiveness should be considered.

Many experimental and numerical investigations have been performed for diffused exit shaped holes to analyze the cooling efficiency and the aerodynamic loss. Gritsch et al. [2] performed an experimental study to investigate the impact of various hole geometric variables on film-cooling performance for fan shaped film-cooling holes. They reported that the area ratio (ratio of cross sectional areas at hole exit and inlet), the hole coverage (the ratio of hole exit width and hole pitch) and the compound angle have little impact on the film-cooling effectiveness, and the film-cooling effectivenesses for the pitch to diameter ratio of 6 and 8 are almost same and better than the pitch to diameter ratio of 4. Saumweber and Schulz [3] investigated the effects of the expansion angle of the diffuser, the inclination angle of the hole, and the length of the cylindrical part at the entrance of fan-shaped and cylindrical holes. Gritsch et al. [4] conducted an experimental investigation to determine the effects of hole geometry and cross-flow Mach number for a cylindrical hole and two holes with a diffuser-shaped exit portion on film-cooling performance. Saumweber and Schulz [5] investigated the cooling performance of cylindrical and fan-shaped holes in a wide range of boundary conditions and reported that separation at the diffuser side-wall significantly degrades performance under high pressure ratios across the hole. Walters and Leylek [6] undertook numerical and experimental investigations of the flow field with cylindrical holes by analyzing vertical motions. From measurements on a range of the L/D ratio of 1.75 to 18, Lutum and Johnson [7] reported that film-cooling effectiveness generally decreased with decreasing L/D when the ratio was less than 5.0 but showed no significant change for L/D that exceeded 5.0. Bunker [8] examined the origins of the shaped film-cooling hole and summarized the extant literature regarding the performance of such film holes. In order to evaluate the performance and characteristics of various hole-shapes, many numerical studies have been conducted, e.g., by Bohn and Moritz [9], Hyams and Leylek [10], Azzi and Jubran [11], Miao and Wu [12], Leedom and Acharya [13] and Mahmood et al. [14]. Day et al. [15] presented a method to define the aerodynamic loss for a film-cooled annular cascade, and a simple mixing model was suggested to analyze the loss contribution for the case of compressible flow and heterogeneous gases. Sargison et al. [16] reported the thermal and aerodynamic performance for the novel console hole and other conventional film cooling hole. Walters and Leylek [17] documented a numerical investigation of the aerodynamic impact of film cooling on a turbine airfoil cascade with single row injection hole. Their numerical results were compared to experimental data in terms of total pressure loss downstream of the blade row, and they reported that the computational methods can be used to predict losses accurately. And, as the study for optimization of film-cooling hole shape, Lee and Kim [18, 19, 20, 21] reported single- and multi-objective optimization works using surrogate modeling for diffused exit shaped hole. As mentioned above, the effects of various parameters on the film cooling effectiveness and the aerodynamic loss have been tested by many experimental and numerical works. However, design optimization simultaneously considering film-cooling effectiveness and aerodynamic loss for a row of holes has not been performed yet.

Engineering design generally involves multiple disciplines and the simultaneous optimization of multiple objectives that are each related to a discipline. These design problems are usually known as multi-objective problems and require simultaneous consideration of all objective functions to enhance the performance of the system. A complete analysis via a full model to explore the possible combinations of the objective functions is always time-consuming and expensive but obviously more accurate than approximate models. In the domain of the approximate analysis of performance, surrogate models have been used to approximate the performance objectives to speed up the design process [22]. Evolutionary algorithms coupled with surrogate analysis [23, 24] have been recently applied to numerically optimize engineering designs. Computational economy and fidelity of the surrogate model in predicting the nature of the design space are two competing considerations. The simultaneous analyses of the design space by the use of multiple surrogate models increase the fidelity of the trust region in the design space. Several algorithms and solution methods are available for solving multi-objective optimization problems [25]. A multi-objective optimization problem consists of many optimal solutions called Pareto-optimal solutions; therefore, a designer's aim is to find as many optimal solutions within the design range as possible. This helps the designer to find a global Pareto-optimal front. Each design set that corresponds to an optimal solution represents a compromise of design objectives. A review of multi-objective optimization methods for engineering was presented by Marler and Arora [26]. A hybrid multi-objective evolutionary algorithm (hybrid MOEA) using elitist Non-dominated Sorting Genetic Algorithm (NSGA-II) combined with a local search strategy [27] has been applied in various engineering-design optimizations including cooling channels [28] and microchannel heat sinks [29, 30]. The shape optimization of a hydraulic turbine diffuser was performed through multi-objective optimization by Marjavaara et al. [31], who applied a local re-sampling scheme.

In the present study, a laidback fan shaped film-cooling hole has been numerically formulated using Reynolds-averaged Navier-Stokes (RANS) analysis, and shape optimization of a row of laidback fan shaped holes considering the film-cooling

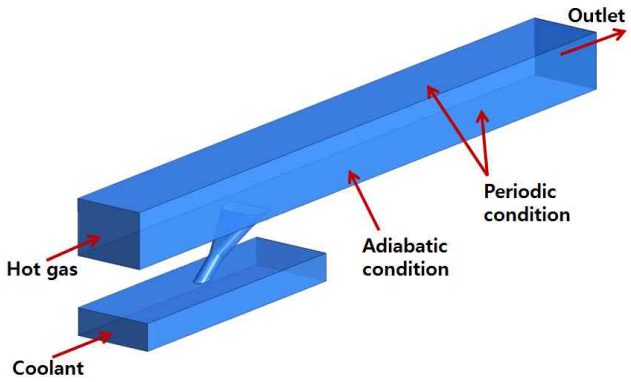

Figure 1: Computational domain and boundary conditions

effectiveness and aerodynamic loss has been performed using hybrid MOEA. A set of optimal designs are presented by Pareto optimal solutions. The trade-off between the two objective functions has been explored and discussed with respect to the design variables.

NUMERICAL ANALYSIS

Fig. 1 shows the laidback fan-shaped hole geometry and computational domain. The computational domain is composed of a main channel of hot gas stream, a coolant channel, and a fan-shaped film cooling hole. Diameter of the cylindrical part of the hole (D) is 10 mm.

To analyze turbulent flow and film-cooling, 3-D Reynolds-averaged Navier-Stokes (RANS) analysis has been performed using ANSYS-CFX 11.0 [32] which employ unstructured grid system. The solutions are obtained by using the finite volume method to discretize the compressible RANS equations. The shear stress transport (SST) turbulence model [33] is used as a turbulence closure. The SST model works by solving a turbulence/frequency-based model (k-ω) near the wall and k-ε model in the bulk flow. A blending function ensures a smooth transition between the two models. Bardina et al. [34] showed that the SST model more effectively captures flow separation under an adverse pressure gradient than other eddy viscosity models, and thus more precisely predicts the near-wall turbulence that plays vital role in the prediction of turbulent heat transfer.

An example of the unstructured hexahedral grid system used in this work is shown in Fig. 2. The grids are concentrated at the wall region to resolve the high velocity gradient. O-type grids are used in the hole. Near the wall, first grid points are placed at $y+$ less than 2 so that low-Re SST model can be implemented properly.

The working fluid is ideal gas (air). In terms of the boundary conditions, adiabatic and no-slip conditions are used at the walls, and constant mass flow rate at inlet of the cooling channel, total pressure at inlet of the main channel, and static pressure at outlet of the main channel are specified. And,

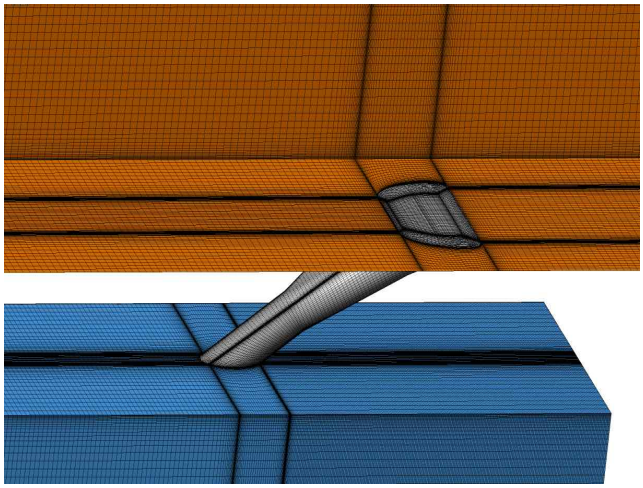

Figure 2: Example of computational grids

periodic conditions are applied to side-to-side surfaces of main channel. In order to adjust Mach number of hot gas in the main channel to the experimental condition [3], 0.3, the velocity at the inlet of main channel is set 130 m/s. Total temperatures of hot gas and coolant are 540K and 290K, respectively. Turbulence intensity in the main channel is 5.2 % and Reynolds number based on the hole diameter is 25,000.

RMS residual values of all flow parameters below 1.0E-5 and energy and mass imbalances in the entire computational domain less than 0.001% were employed as the convergence criteria. And, the changes of objective function values measured (uncertainty) were less than 5.0E-4. The solver finished a single simulation in approximately 1000 iterations. The computations were performed by an Intel I7 CPU 960, and each calculations was subdivided into 8 tasks performing the data transfer using the MPICH2 local parallel. The computational time per a single simulation was typically 10~12 hours, and the time of computation depends on geometry considered.

DESIGN VARLIABLES AND OBJECTIVE FUNCTIONS

The previous numerical optimization works [19, 20, 21] were performed on a single film hole design. However, in the application of film-cooling on gas turbine blades, film-cooling is typically applied by means of rows of film holes, and the effect of hole-to-hole interaction should be considered. In the present optimization, therefore, four geometric variables, viz., the injection angle of the hole (α), the lateral expansion angle of the diffuser (β), the forward expansion angle of the hole (γ), and the ratio of the pitch to the diameter of the hole (P/D) shown in Fig. 3, are selected as design variables. As reported in the previous studies [19, 20], the length to diameter ratio (L/D) has less impact than the other geometric variables, and the optimum spatially averaged film-cooling effectiveness occurs around L/D=7. Therefore, L/D was fixed at 7 in the present optimization, and the wall thickness has been changes as the

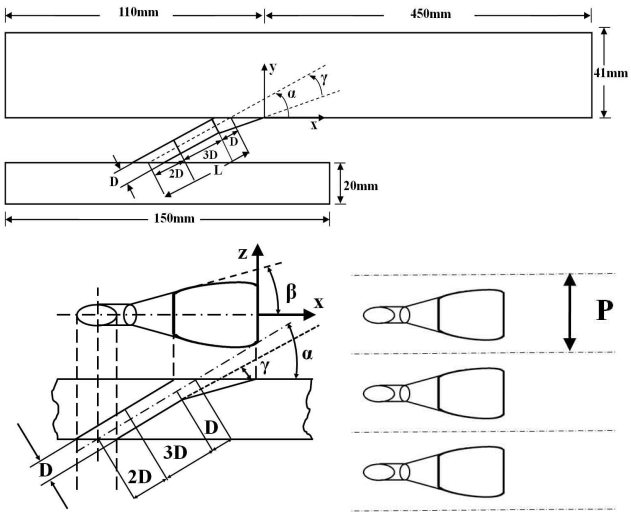

Figure 3: Geometric variables of laidback fan shaped film-cooling hole

Table 1: Design variables and design space

Design variables	Lower bound	Upper bound
α (°)	25	45
β (°)	10	21
γ (°)	0	10
P/D	5	8

injection angle. The design space which is constituted by the lower and upper limits of the variables is shown in Table 1. The ranges of design variables are set considering the results of the previous numerical works [19, 20]. Before deciding the final ranges of variables, it is checked that the lower and upper limits of the variables produce feasible geometries during design of experiments (DOE).

To maximize the performance of the film-cooling hole, two objective functions F_{FCE} and F_{AL} based on film-cooling effectiveness and aerodynamic loss, respectively, are selected. The main motive of the optimization is to minimize both of the objective functions, F_{FCE} and F_{AL}.

F_{FCE} is defined as a reciprocal of spatially averaged film-cooling effectiveness normalized by D/P (eq. 1). It is expectable result that small P/D provides a higher film-cooling performance in comparison with high P/D because the small P/D at same blowing ratio means use of large amount of coolant as compared to higher P/D. Therefore, the film-cooling effectiveness normalized by D/P is used so that the film-cooling performance of the experimental designs which have different P/D can be fairly evaluated. Gritch et al. [2] also used same way to evaluate the effect of P/D. And, in film-cooling, primary concern is not only how high the film-cooling effectiveness is but also how much the film left downstream of the hole. Therefore, the spatially averaged film-cooling effectiveness is averaged over an area in 40 hole diameters in the steamwise length, and defined as follows:

$$F_{FCE} = \frac{1}{\eta_S / (D/P)} \tag{1}$$

$$\eta_S = \frac{1}{P \times 40} \int_0^P \int_0^{40} \eta(x/D, z/D)\, d(x/D)\, d(z/D) \tag{2}$$

$$\eta(x/D, z/D) = \frac{T_{aw}(x/D, z/D) - T_\infty}{T_c - T_\infty} \tag{3}$$

where T_{aw} adiabatic wall temperature, and T_∞ and T_c are free-stream temperature in the main channel and coolant jet temperature, respectively.

Another objective function, F_{AL} is formulated as follows [15, 16]:

$$F_{AL} = \left(1 - \frac{KE_{Actual}}{KE_{Theoretical}}\right) / (D/P) \tag{4}$$

KE_{Actual} and $KE_{Theoretical}$ mean the actual and theoretical kinetic energy flux, respectively, at the mixing plane. The mixing plane is defined as the hypothetical plane at which the coolant and mainstream flows are fully mixed and the velocity, pressure and temperature are uniform. It is mathematically equivalent to the measurement plane and the velocity, static pressure and temperature at this plane are found by applying the laws of conservation of mass, momentum and energy between the reference plane and the mixing plane [16]. And, this term is also normalized by a reciprocal of P/D. Although this measurement is dependent on the dimensions of main channel, the purpose of the current measurement is to generate comparative data only.

Applying conservation of mass from the reference plane to the mixing plane shown in Fig. 4,

$$V_2 = \frac{\iint_{A_m} V dy dz}{A_m} \tag{5}$$

Here, A_m and V are the area of main channel and flow velocity, respectively. And, applying conservation of momentum,

$$p_2 = p_1 + \rho \iint_{A_m} V^2 dy dz - \rho A_m V_2^2 \tag{6}$$

From eq. (5) and (6), KE_{Actual} can be calculated as follows:

$$KE_{Actual} = \frac{1}{2} \rho_2 V_2^3 \tag{7}$$

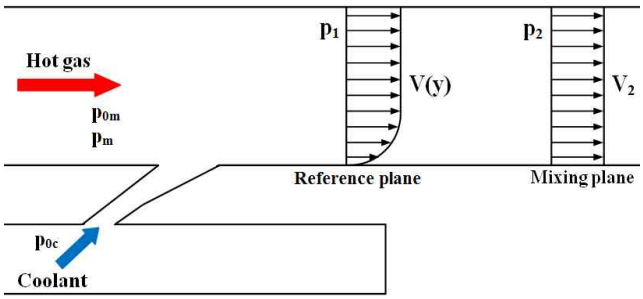

Figure 4: Reference and mixing planes for aerodynamic loss

The theoretical kinetic energy flux, $KE_{Theoretical}$, is calculated from the initial total pressure and static pressure at the mixing plane as follows:

$$KE_{Theoretical} = \frac{m_m}{\rho_m}(p_{0m} - p_2) + \frac{m_c}{\rho_c}(p_{0c} - p_2) \quad (8)$$

where p_{0m} and p_{0c} are total pressure of main channel and coolant plenum, respectively, and m_m and m_c are mass flux of main flow and coolant, respectively.

OPTIMIZATION TECHNIQUES

Surrogate construction

Multi-objective optimization that is based on evolutionary algorithms requires a large number of evaluations of objective functions to search for the optimal solutions. The number of evaluations of the objective functions could be of the order of thousands depending upon the parameters of the genetic algorithm (generally greater than $N_p \times N_g$). Here N_p is the size of population and N_g is the number of generations. Therefore a full numerical model optimization is not feasible in view of the required computational time and expenses for these evaluations. Therefore, to evaluate these objective function values, surrogate based approximation is utilized to avoid numerical or experimental expense and save time. Queipo et al. [22] suggested the application of various surrogate models, including Response Surface Approximation and Kriging meta-modeling. In the present study, the Kriging model is applied to evaluate objective function values at the required design sites.

The Kriging (KRG) model [35] is an interpolating meta-modeling technique that employs a trend model, $F(\boldsymbol{x})$, to capture large-scale variations and a systematic departure, $Z(\boldsymbol{x})$, to capture small-scale variations. Kriging postulation is the combination of a global model and departures of the following form:

$$f(x) = F(x) + Z(x) \quad (9)$$

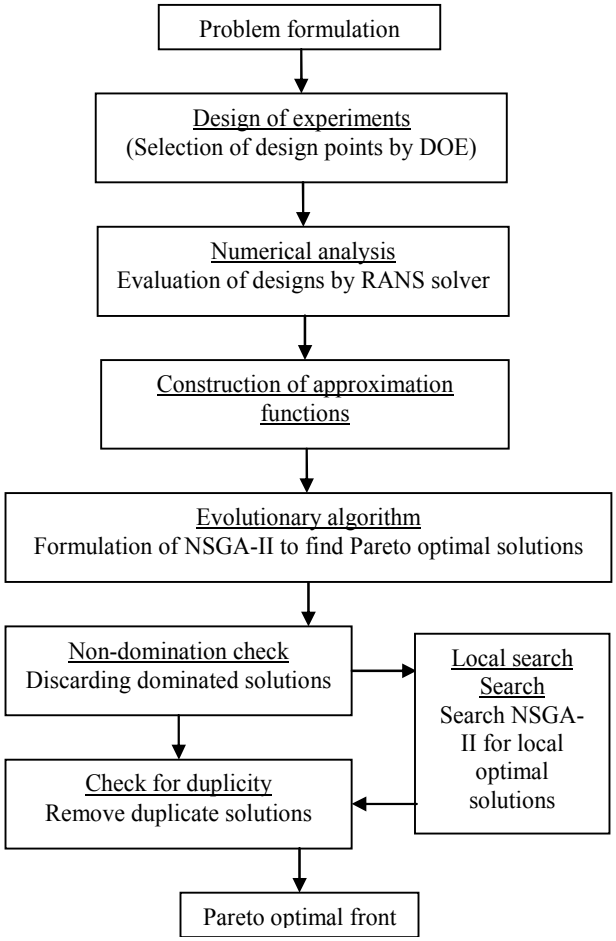

Figure 5: Multi-objective optimization procedure

In Eq. (9), $f(x)$ represents the unknown function and $F(x)$ is the global model, while $Z(x)$ represents the localized deviations. $Z(x)$ is the realization of a stochastic process with zero mean and non-zero covariance. A linear polynomial function is used as a trend model and the systematic departure terms follow a Gaussian correlation function.

Multi-Objective Evolutionary Algorithm

A multi-objective optimization problem stated above is formulated as:

$$\begin{aligned} &\text{Minimize} && \bar{f}(\bar{x}) \quad \text{(M functions to be optimized)} \\ &\text{Subject to} && \bar{g}(\bar{x}) \le 0 \quad \text{(s inequality constraints)} \\ & && \bar{h}(\bar{x}) = 0 \quad \text{(t equality constraints)} \end{aligned}$$

where $\bar{f}(\bar{x}) = \left\{\bar{f}_1(\bar{x}), \bar{f}_2(\bar{x}), \bar{f}_3(\bar{x}), \ldots\ldots \bar{f}_M(\bar{x})\right\}$ is a vector of M real-valued objective functions, and x is a vector of N design

variables. Thus, $\bar{x} \in R^N$, $\bar{g}(\bar{x}) \in R^s$, $\bar{h}(\bar{x}) \in R^t$. The present problem is associated with two competing objectives in which improvement of one objective leads to deterioration of other objective. Each feasible solution set $\bar{x}$ of multi-objective problem is either dominated or non-dominated, in which all non-dominated solutions are called Pareto optimal solutions. Vector $\bar{x}_i$ dominates a vector $\bar{x}_j$ if $\bar{x}_i$ is at least as good as $\bar{x}_j$ for all objectives and $\bar{x}_i$ is strictly better than $\bar{x}_j$ for at least one objective.

The methodology used to generate global Pareto optimal solutions (POSs) is shown in Fig. 5. Objective functions are defined mathematically and evaluated on the data obtained by numerical simulation. A hybrid multi-objective evolutionary approach is used to obtain global Pareto optimal solutions. In this method, first, approximate Pareto optimal solutions are obtained using real coded NSGA-II developed by Deb et al. [25] for two objective functions based on film-cooling effectiveness and aerodynamic loss. Here, real coded means that the crossover and mutations are conducted in real space to obtain a response of NSGA-II. In this method the selected size (say P_n) of the population, which is called parent population, is first randomly initialize and objective functions are computed at each design. Here population means designs in the design space. The Rank of this population is then obtained based on the non-domination criteria and crowding distance. A genetic operator is applied to create intermediate population of size P_n through selection, crossover and mutation. The objective functions are evaluated for the intermediate population, and the two populations (parent and intermediate) are combined. The Rank of the combined population is obtained and crowding distance is evaluated. Based on the rank and crowding distance new population of P_n best individuals is selected from the combined population. This new population is again ranked for the next generation based on the non-domination criteria and the procedure is repeated till the limiting number of generations is reached.

These solutions are then refined by searching a local optimal solution for each objective function over the whole NSGA-II obtained optimal solutions using Sequential Quadratic Programming (SQP) [36] with NSGA-II solutions as initial guesses. SQP is a generalization of Newton's method which is gradient based optimization technique. To perform local search usually two approaches are applied [25]. In one approach all the objectives are combined into a single composite objective and optimum is searched. In another approach one objective is optimized treating the others as equality constraints and the process is repeated to all objectives. In the present study first objective is optimized and second objective is treated as equality constraint. The local search is repeated for second objective function treating the first as equality constraint. This process gives two new sets of optimal solutions which are then merged with the NSGA-II solutions. From these solutions, dominated solutions are discarded and then duplicate solutions are removed to get global Pareto optimal solutions. The process of local search improves the quality of Pareto optimal solutions.

***K*-means clustering**

In order to find out representative solutions from the POSs, K-mean clustering [37] was performed. The representative optimal points obtained by the local search are grouped into three clusters applying *K*-means clustering algorithm. It is an iterative alternating fitting process to form the number of specified clusters. These clusters are distributed uniformly along the POSs.

RESULTS AND DISCUSSION

The grid independency test and validation of computational results were performed and reported in the previous studies by Lee and Kim [19, 20].

The present multi-objective optimizations have been performed for the two blowing ratios, 0.5 and 2.0. And, the film-cooling hole shape is optimized in terms of four design variables, α, β, γ, and P/D, for blowing ratios of 0.5 and 2.0, respectively. The design space shown in Table 1 was first explored by preliminary calculations under geometric and flow constraints and decided on the basis of prior numerical studies [19, 20]. The objective functions which are defined as the spatially averaged film-cooling effectiveness and the aerodynamic loss were numerically evaluated through RANS analysis at 40 experimental points that are selected through the Latin hypercube sampling (LHS) method within the design spaces. Using these data, KRG model was constructed, and the global Pareto optimal solutions were obtained by hybrid MOEA. A real-coded NSGA-II was invoked to obtain well-spread, approximate Pareto-optimal solutions with 150 generations and 100 populations. The crossover and mutation probabilities were set to 0.85 and 0.15, respectively. The crossover and mutation parameters were decided as 15 and 150, respectively. These parameters were adjusted one-by-one to suit the nature of the problem.

Pareto optimal solutions (POSs) and the experimental designs for the blowing ratios of 0.5 and 2.0 are shown in Figs. 6(a) and (b), respectively. The solutions represent all the optimal designs obtained by hybrid MOEA. Since both the objective functions are being minimized, the obtained Pareto optimal solutions resemble a concave front and for every fixed value of one objective function, there is one optimal value of the other objective function. Each extreme end of the Pareto optimal solution represents a pair of the lowest value of one objective function and the highest value of the other objective function. Any improvement of one objective function leads to the deterioration of the other objective function; this shows the competing nature of the two objective functions. Here, it can be observed that no solution

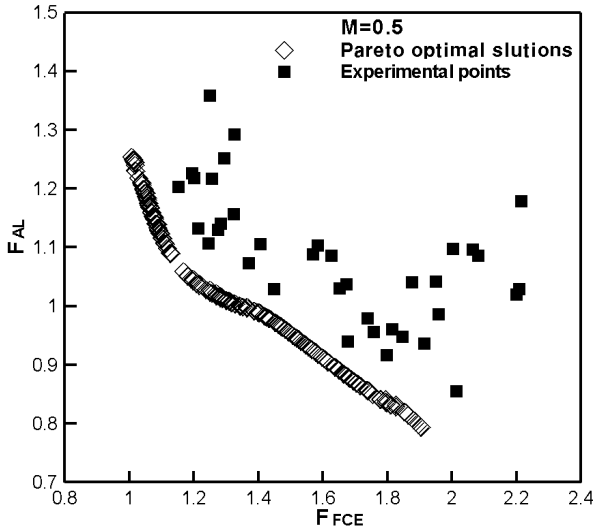

(a) M=0.5

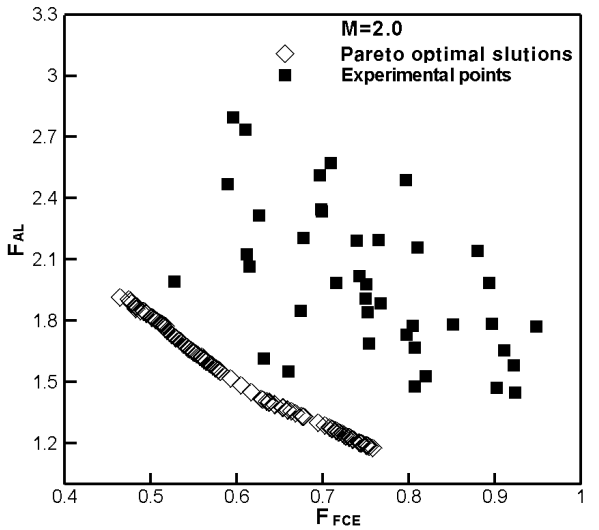

(b) M=2.0

Figure 6: Pareto optimal solutions using hybrid MOEA and the experimental designs

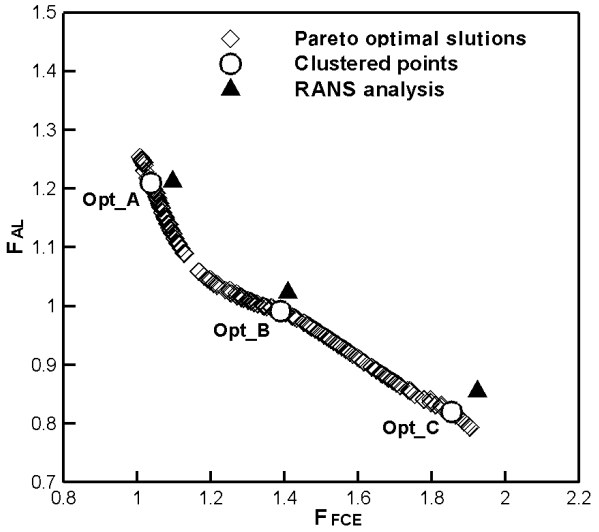

(a) M=0.5

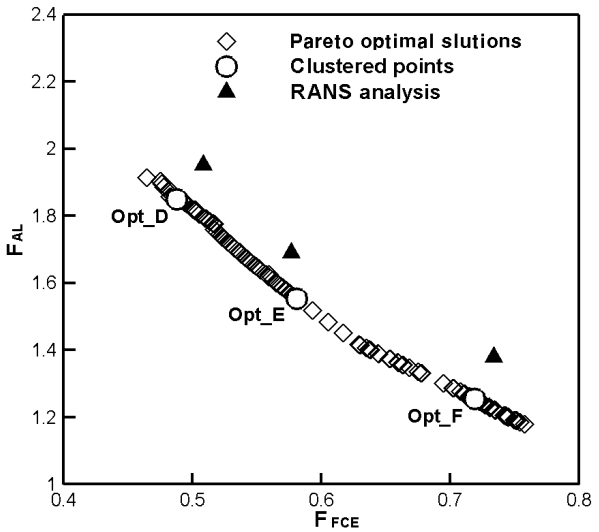

(b) M=2.0

Figure 7: Clustered points and corresponding results through RANS analysis

out of these POSs is superior to any other solution in both objectives.

Figs. 7 (a) and (b) show the six clustered points from the Pareto optimal solutions for blowing ratios of 0.5 and 2.0, respectively. And, the optimum geometries are shown in Fig. 8. The six optimum designs (Opt_A, B, C, D, E and F) are obtained by *K*-means clustering. And, these optimal designs are evaluated by RANS analysis. The Opt_A and Opt_D represent the high film-cooling effectiveness and high aerodynamic loss. On the other hand, the Opt_C and Opt_F show the low film-cooling effectiveness and low aerodynamic loss. Hence, the designer can select any optimum design from the POSs according to their needs.

Tables 2 and 3 show the optimization results for the optimal designs clustered from the POSs as well as a comparison with a reference geometry which has been selected

Table 2: Comparison of the predicted and RANS calculated values at the optimal designs (M=0.5)

Shapes	Design variables				Predicted value by hybrid MOEA		RANS calculated value	
	α (°)	β (°)	γ (°)	P/D	F_{FCE}	F_{AL}	F_{FCE}	F_{AL}
Reference	37.31	19.31	7.949	5.846	-	-	1.585	1.149
Opt_A	44.87	18.99	1.052	7.826	1.037	1.209	1.096	1.212
Opt_B	34.07	16.87	4.820	6.042	1.389	0.991	1.409	1.023
Opt_C	27.62	13.43	8.924	5.162	1.854	0.819	1.924	0.855

Table 3: Comparison of the predicted and RANS calculated values at the optimal designs (M=2.0)

Shapes	Design variables				Predicted value by hybrid MOEA		RANS calculated value	
	α (°)	β (°)	γ (°)	P/D	F_{FCE}	F_{AL}	F_{FCE}	F_{AL}
Reference	37.31	19.31	7.949	5.846	-	-	0.601	2.102
Opt_D	26.02	20.78	2.291	6.936	0.488	1.849	0.508	1.950
Opt_E	33.61	16.04	5.890	6.052	0.581	1.552	0.577	1.689
Opt_F	43.15	13.86	9.854	5.033	0.719	1.254	0.734	1.378

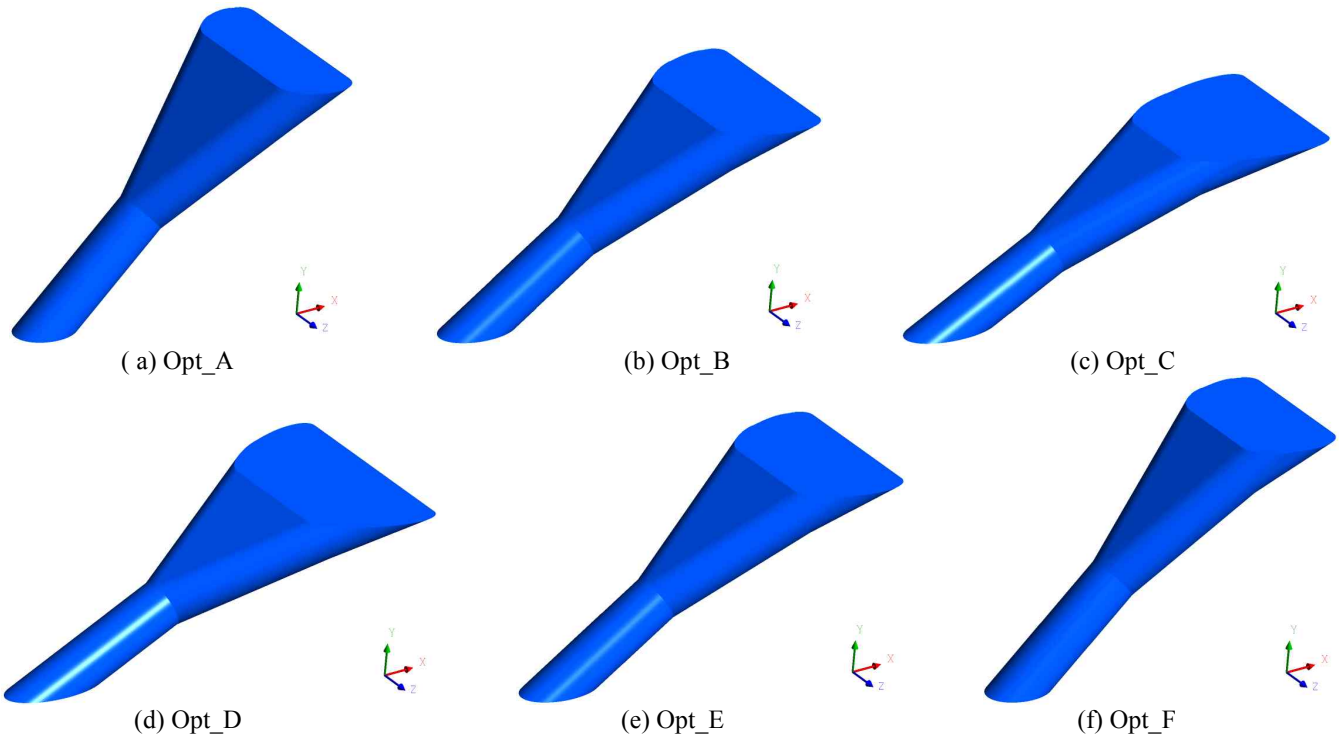

(a) Opt_A (b) Opt_B (c) Opt_C

(d) Opt_D (e) Opt_E (f) Opt_F

Figure 8: Optimal film-cooling hole geometries

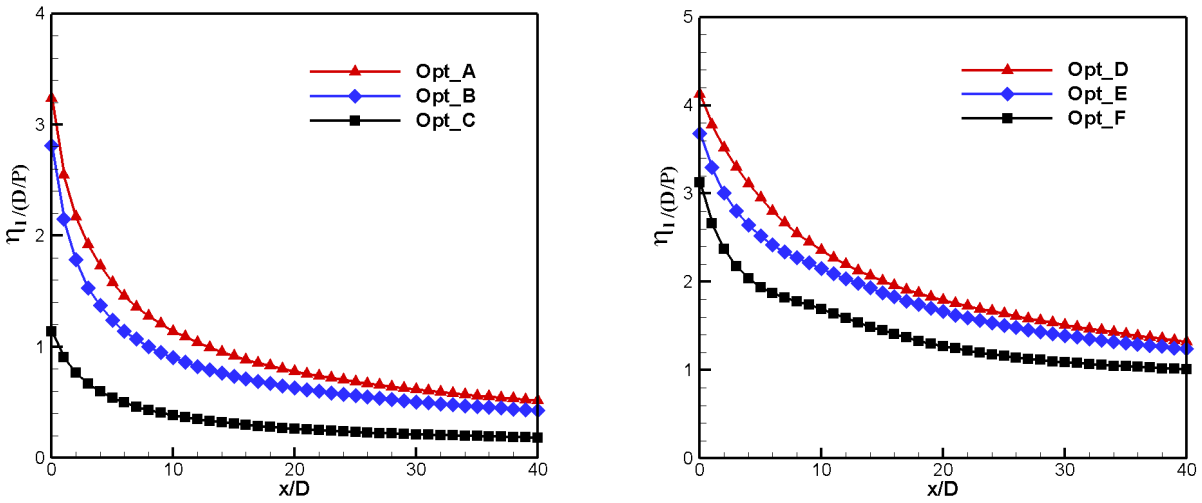

(a) M=0.5 (b) M=2.0

Figure 9: Laterally averaged film-cooling effectiveness for optimal designs

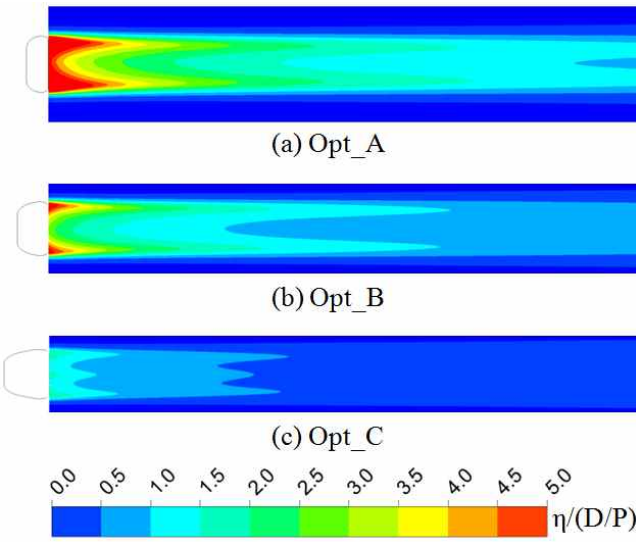

Figure 10: Film-cooling effectiveness for M=0.5

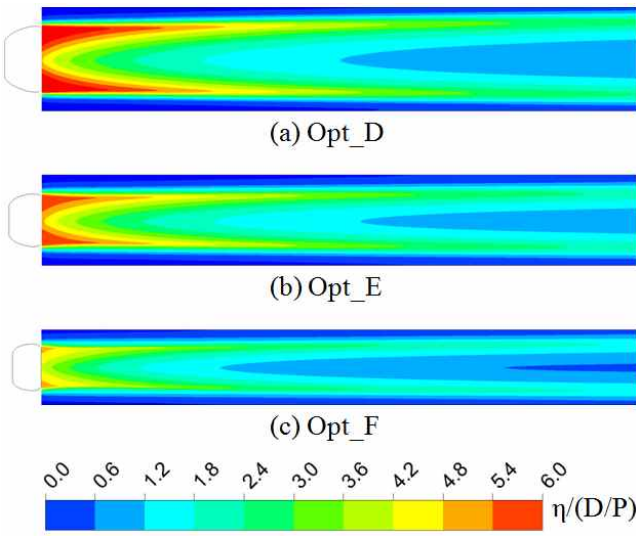

Figure 11: Film-cooling effectiveness for M=2.0

arbitrarily in the design space. The objective function values predicted by hybrid MOEA agree with the values obtained by RANS analysis with relatively errors in the range, 1.0% ~ 8.3%. As the optimization results for the blowing ratio of 0.5 represented in Table 2, the increase in α, β and P/D and the decrease in γ produce higher film-cooling effectiveness and less aerodynamic loss. In comparison with the reference shape, the Opt_A shows higher film-cooling effectiveness and the Opt_C represents lower aerodynamic loss. The Opt_B shows enhanced performances on both the objectives. For the optimal designs at the blowing ratio of 2.0 shown in Table 3, the values of β, γ and P/D show same trend with the optimization results for M=0.5. However, the injection angle (α) shows quit contrary trend when compared with the results for the blowing ratio of 0.5. The Opt_D and Opt_E show better performance on film-cooling effectiveness as well as on aerodynamic loss, and the Opt_F represents much lower aerodynamic loss in comparison with the reference geometry. In conclusion, the Opt_B and Opt_E can be considered to represent the global optimum geometry because the optimum designs are very similar and show higher performances on the objectives regardless the blowing ratio.

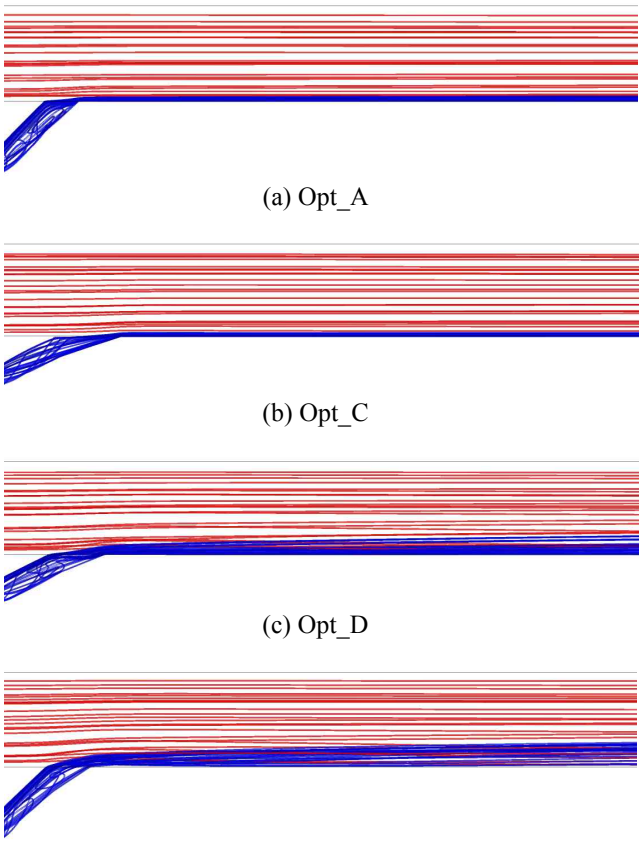

(a) Opt_A

(b) Opt_C

(c) Opt_D

(d) Opt_F

Figure 12: Streamlines of mainstream and coolant for optimal designs

Fig. 9 shows a comparison of laterally averaged film-cooling effectiveness normalized by D/P for the optimal designs. The Opt_A and Opt_D give higher film-cooling effectiveness than the other optimal designs through the downstream region of the film-cooling hole.

The contours of the local film-cooling effectiveness on the film-cooling surface for the blowing ratios of 0.5 and 2.0 are shown in Figs. 10 and 11, respectively. The optimal designs yield similar contour shapes except Opt C shows three peaks, but large quantitative differences. The Opt_A and D show a larger region of high film-cooling effectiveness due to improved lateral spreading of the coolant.

Fig. 12 shows streamlines of mainstream (red lines) and coolant (blue lines) for the Opt_A, C, D and F. In the optimal designs for low blowing ratios (Opt_A and C), it can be seen that the coolant coming out from the hole flows close to cooling surface regardless the injection angle of the hole (α) due to low momentum of the coolant. On the other hand, the results for high blowing ratio (Fig. 11(c) and (d)) indicate that the coolant flow shows different behavior according to the injection angle. The coolant jet in the Opt_F penetrates into the mainstream more deeply as compared to the Opt_D which has lower injection angle than that of the Opt_F.

Table 4: Hole width to pitch ratio and area ratio for optimal designs

	W/P	AR
Opt_A	0.5349	4.6508
Opt_B	0.6019	4.9149
Opt_C	0.6409	5.3685
Opt_D	0.6363	5.4022
Opt_E	0.6228	4.9485
Opt_F	0.6233	4.8666

Fig. 13 represents the normalized turbulence kinetic energy (K/U_∞) distributions on y-z planes at x/D=0.5 and 2.0 for the Opt_A, B and C. For the Opt. A, relatively higher turbulence intensity is generated in the wider region which causes higher heat transfer performance but with higher aerodynamic loss in comparison with the Opt_B and C.

The width at hole exit side to hole pitch ratio (W/P) and the ratio of the areas at hole exit and inlet (AR) for the six optimal designs are tabulated in Table 4. The W/P is frequently assumed to describe the potential of the coolant to spread out laterally and form a self-contained film with the coolant emerging from its neighbor holes. And, the AR was measured to evaluate the effect on the film-cooling effectiveness. Low momentum of the coolant coming out the hole exit leads to less penetration into the main hot gas, and induces higher film-cooling effectiveness [2]. In the optimal designs for blowing ratio of 0.5, as the W/P increases from 0.53 to 0.64, the area-averaged film-cooling effectiveness decreases and the aerodynamic loss also decreases. At the blowing ratio of 2.0, on the other hand, the optimal designs have the almost same values of W/P as shown in Table 4. Taking a looking at the AR values for the optimal designs represented in Table 4, the AR values are found to be in the range of 4.7 to 5.4. And, higher AR gives lower film-cooling effectiveness and less aerodynamic loss at the low blowing ratio (M=0.5). However, for the higher blowing ratio (M=2.0), the reverse trend is found as higher AR makes higher film-cooling effectiveness and higher aerodynamic loss. Although the data tabulated in Table 4 show different trend of variations of the W/P and AR between the optimum geometries for the blowing ratios of 0.5 and 2.0, the W/P and AR for the optimal designs are found to be in small ranges, 0.53-0.64 and 4.7-5.4, respectively. Therefore, it can be a guideline for design of film-cooling hole.

Fig. 14 shows the film-cooling effectiveness distributions on the film-cooling surface and turbulence kinetic energy distributions on the y-z planes at x/D=20 and 40 for the reference geometry and the Opt_D. The reference geometry has smaller pitch (W/P=0.701) as compared to the Opt_D as shown

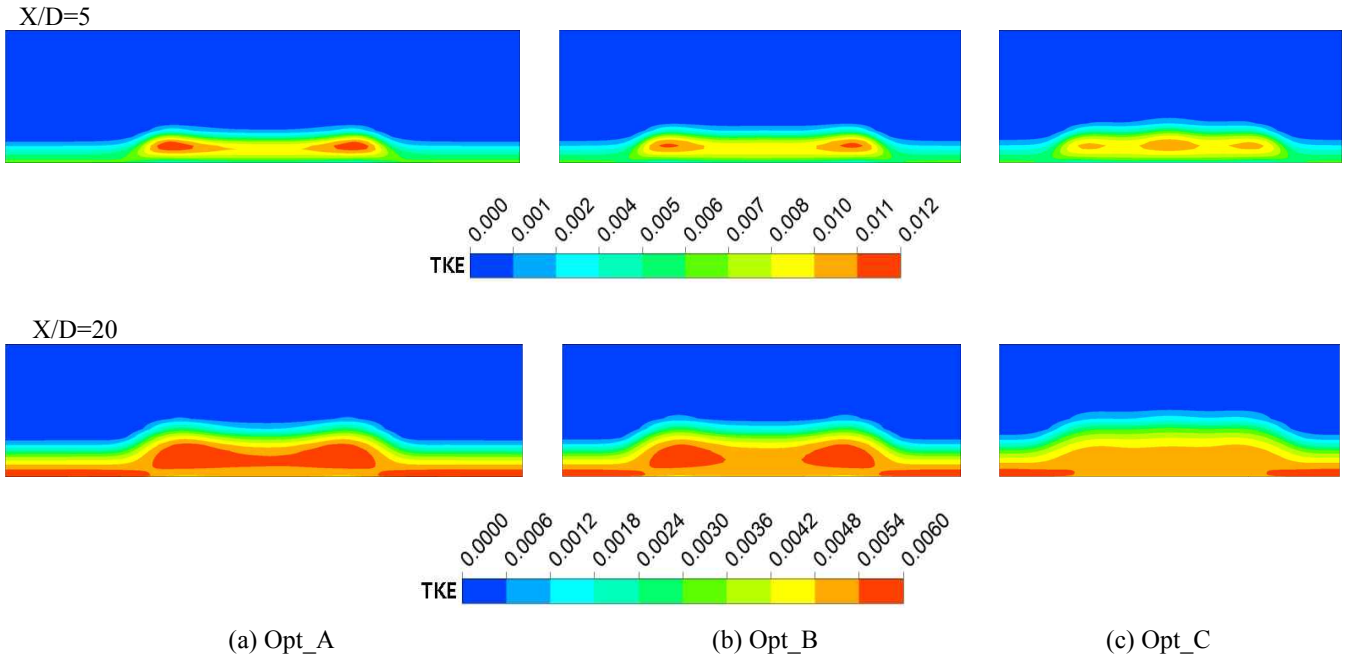

(a) Opt_A (b) Opt_B (c) Opt_C

Figure 13: Turbulence kinetic energy (K/U_∞) distribution on y-z plane

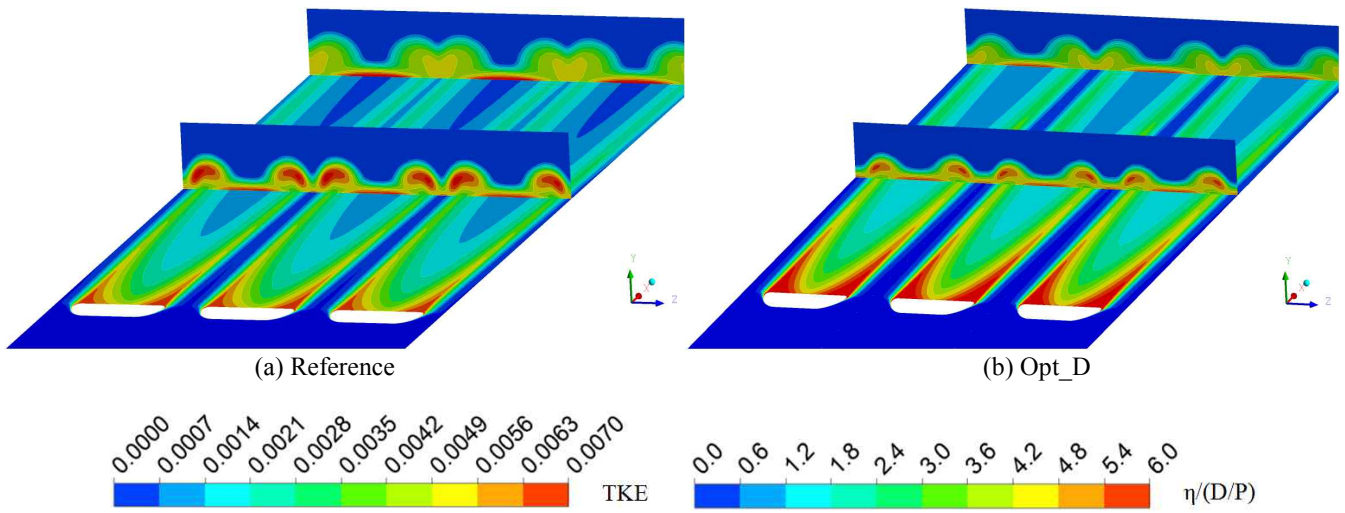

(a) Reference (b) Opt_D

Figure 14: Film-cooling effectiveness on the cooling surface and turbulence kinetic energy distributions on y-z planes (x/D=20 and 40) for M=2.0

in Tables 2 and 3. As shown in this figure, the reference shape shows the generations of stronger vortices and higher turbulence intensity due to intensified interaction between the coolants from the adjacent cooling holes. This results in a decrease of film-cooling effectiveness as well as an increase of aerodynamic loss.

CONCLUSION

Multi-objective optimization of laidback fan-shaped holes has been carried out to enhance the film-cooling effectiveness compromising with the aerodynamic loss with four design variables, viz., the injection angle of the hole, the lateral expansion angle of the diffuser, the forward expansion angle of the hole, and the ratio of the pitch to diameter of the hole. The KRG method and hybrid multi-objective evolutionary algorithm

have been used for the optimization. The objective functions have been calculated by three-dimensional RANS analysis at the design points selected by LHS method. Design optimizations have been performed for both low and high blowing ratios, i.e., 0.5 and 2.0, respectively. Both film-cooling effectiveness and aerodynamic loss based objectives are optimized, and a set of optimum designs have been presented by POSs. Three optimum designs from POSs for each blowing ratio have been selected and analyzed. Both of the optimal designs for the blowing ratios of 0.5 and 2.0, commonly show that the increase in β and P/D and the decrease in γ produce higher film-cooling effectiveness and less aerodynamic loss. In the case of α, however, quite contrary trend is found between the sets of optimal designs for the high and low blowing ratios. The W/P and AR for the optimal designs are found to be in small ranges, 0.53-0.64 and 4.7-5.4, respectively. And, the higher AR gives the lower film-cooling effectiveness and the less aerodynamic loss at the lower blowing ratio (M=0.5), and vice versa for the higher blowing ratio (M=2.0). The present multi-objective optimization techniques provide an efficient design tool for engineering problem without extreme error rate, and it is expected for designers to meet their design requirement from the POSs.

ACKNOWLEDGMENTS

This research was supported by the National Research Foundation of Korea (NRF) Grant No. 20090083510 funded by government (MEST) through Multi-phenomena CFD Engineering Research Center.

REFERENCES

[1] Goldstein, R. J., Eckert, E. R. G., and Burggraf, F., 1974, "Effects of Hole Geometry and Density on Three-Dimensional Film Cooling," Int. J. Heat Mass Transfer, Vol. 17, pp. 595-607.

[2] Gritsch, M., Colban, W., Schar, H., and Dobbeling, K., 2005, "Effect of Hole Geometry on the Thermal Performance of Fan-Shaped Film Cooling Holes," ASME Journal of Turbomachinery, Vol. 127, pp. 718-725.

[3] Saumweber, C., and Schulz, A., 2008, "Effect of Geometry Variations on the Cooling Performance of Fan-Shaped Cooling Holes," ASME Turbo Expo 2008, Berlin, GT2008-51038.

[4] Gritsch, M., Schulz, A., and Wittig, S., 1998, "Adiabatic Wall Effectiveness Measurements of Film-Cooling Holes With Expanded Exits," ASME Journal of Turbomachinery, Vol. 120, pp. 549-556.

[5] Saumweber, C., and Schulz, A., 2008, "Free-Stream Effects on the Cooling Performance of Cylindrical and Fan-Shaped Cooling Holes," ASME Turbo Expo 2008, Berlin, GT2008-51030.

[6] Walter, D. K., and Leylek, J. H., 2000, "A Detailed Analysis of Film-Cooling Physics: Part1-Streamwise Injection with Cylindrical Holes," ASME Journal of Turbomachinery, Vol. 122, pp.102-112.

[7] Lutum, E., and Johnson, B. V., 1999, "Influence of the Hole Length-to-Diameter Ratio on Film Cooling With Cylindrical Holes," ASME Journal of Turbomachinery, Vol. 121, pp. 209-216.

[8] Bunker, R. S., 2005, "A Review of Shaped Hole Turbine Film-Cooling Technology," Journal of Heat Transfer, Vol. 127, pp. 441-453.

[9] Bohn, D., and Moritz, N., 2003, "Numerical Parametric Study on Full Coverage Cooled Multi-Layer Plates," Proceeding of the International Gas Turbine Congress 2003, Tokyo, IGTC2003 Tokyo TS-84.

[10] Hyams, D. G., and Leylek, J. H., 2000, "A Detailed Analysis of Film Cooling Physics: Part3-Streamwise Injection With Shaped Holes," ASME Journal of Turbomachinery, Vol. 122, pp. 122-132.

[11] Azzi, A., and Jubran, B. A., 2007, "Numerical modeling of film cooling from converging slot-hole," Heat Mass Transfer, Vol. 43, pp. 381-388.

[12] Miao, J. M., and Wu, C. Y., 2006, "Numerical approach to hole shape effect on film cooling effectiveness over flat plate including internal impingement cooling chamber," International Journal of Heat and Mass Transfer, Vol. 49, pp. 919-038.

[13] Leedom, D. H., and Acharya, S., 2008, "Large Eddy Simulation of Film Cooling Flow Field From Cylindrical and Shaped Holes," ASME Turbo Expo 2008, Berlin, GT2008-51009.

[14] Mahmood, S., Kassab, A. J., and Divo, E., 2005, "Film Cooling Effectiveness from a Single Scaled-Up Fan-Shaped Hole: A CFD Simulation of Adiabatic and Conjugate Heat Transfer Models," ASME Turbo Expo, Nevada, GT2005-68431.

[15] Day, C. R. B., Oldfield, M. L. G., and Lock, G. D., 2000, "Aerodynamic performance of an annular cascade of film cooled nozzle guide vanes under engine representative conditions," Experiments in Fluids, Vol. 29, pp. 117-129.

[16] Sargison, J. E., Guo, S. M., Oldfield, M. L. G., Lock, G. D., and Rawlinson, A. J., 2002, "A Converging Slot-Hole Film-Cooling Geometry-Part 1: Low-Speed Flat-Plate Heat Transfer and Loss," ASME Journal of Turbomachinery, Vol. 124, pp. 453-460.

[17] Walters, D. K., and Leylek, J. K., 2000, "Impact of Film-Cooling Jets on Turbine Aerodynamic Losses," ASME Journal of Turbomachinery, Vol. 122, pp. 537-545.

[18] Lee, K. D., and Kim, K. Y., 2009, "Optimization of A Fan-Shaped Hole for Film Cooling Using A Surrogate Model," ASME Turbo Expo 2009, Orlando, GT2009-59520.

[19] Lee, K. D., and Kim, K. Y., 2010, "Shape Optimization of A Laidback Fan-Shaped Film-Cooling Hole To Enhance

Cooling Performance," ASME Turbo Expo 2010, Glasgow, GT2010-22398.

[20] Lee, K. D., and Kim, K. Y., 2010, "Shape Optimization of a Fan-Shaped Hole to Enhance Film-Cooling Effectiveness," International Journal of Heat and Mass Transfer, Vol. 53, pp. 2996-3005.

[21] Lee, K. D., Afzal, H., and Kim, K. Y., 2010, "Multi-objective Optimization of a Laidback Fan Shaped Film-Cooling Hole Using Evolutionary Algorithm," International Journal of Fluid Machinery and Systems, Vol. 3, No. 2, pp. 150-159.

[22] Queipo, N. V., Haftka, R. T., Shyy, W., Goel, T., Vaidyanathan, R., and Tucker, P. K., 2005, "Surrogate-based analysis and optimization," Progress in Aerospace Science, Vol. 41, pp. 1-28.

[23] Wilson, B., Cappelleri, D., Simpson, T. W., and Frecker, M., 2001, "Efficient Pareto frontier exploration using surrogate approximations," Optimizaiton and Engineering, Vol. 2, pp. 31-50.

[24] Bramanti, A., Barba, P. D., Farina, M., and Savini, A., 2001, "Combining response surfaces and evolutionary strategies for multiobjective Pareto-optimization in electromagnetic," International Journal of Applied Electromagnetics and Mechanics, Vol. 15, pp. 231-236.

[25] Deb, K., 2001, "Multi-objective optimization using evolutionary algorithms," 1st ed. John Wiley & Sons Inc.

[26] Marler, R. T., and Arora, J. S., 2004, "Survey of multi-objective optimization methods for engineering," Structural and Multidisciplinary Optimization, Vol. 26, No. 6, pp. 369–395.

[27] Goel, T., Vaidyanathan, R., Haftka, R. T., Shyy, W., Queipo, N. V., and Tucker, K., 2007, "Response surface approximation of Pareto optimal front in multi-objective optimization," Comput. Methods Appl. Mech. Engrg., Vol. 196, pp. 879-893.

[28] Li, P., and Kim, K. Y., 2008, "Multiobjective optimization of staggered elliptical pin-fin arrays," Numerical Heat Transfer, Part A, Vol. 53, No. 4, pp. 418-431.

[29] Husain, A., and Kim, K. Y., 2008, "Microchannel heat sink with designed roughness: analysis and optimization.," Journal of Thermophysics Heat Transfer, Vol. 22, No. 3, pp. 342-351.

[30] Husain, A., and Kim, K. Y., 2008, "Multiobjective optimization of a microchannel heat sink using evolutionary algorithm," Journal of Heat Transfer, Vol. 130, No. 11, pp. 114505-1 114505-3.

[31] Marjavaara, B. D., Lundstrom, T. S., Goel, T., Mack, Y., and Shyy, W., 2007, "Hydraulic turbine diffuser shape optimization by multiple surrogate model approximations Pareto fronts," Journal of Fluids Engineering, Vol. 129, No. 12, pp. 1228-1240.

[32] CFX-11.0 Solver Theory, Ansys inc., 2008.

[33] Menter, F., and Esch, T., 2001, "Elements of Industrial Heat Transfer Prediction," 16th Bazilian Congress of Mechnacal Engineering (COBEM), Uberlandia Brazil.

[34] Bardina, J. E., Huang, P. G., and Coakley, T., 1997, "Turbulence Modeling Validation," Fluid Dynamics Conference 28th, AIAA Paper 1997-2121.

[35] Martin, J. D., and Simpson, T. W., 2005, "Use of Kriging Models to Approximate Deterministic Computer Models," AIAA Journal, Vol. 4, pp. 853-863.

[36] MATLAB ®, The language of technical computing, Release 14, The Math Works Inc.

[37] JMP, The Statistical discovery software, version 6, SAS Institute Inc., Cary, NC, USA, 2005.